



Hydroisomerization of long-chain *n*-alkanes over Pt/AlSBA-15 + zeolite bimodal catalysts

Karolina Jaroszewska*, Monika Fedyna, Janusz Trawczyński

Wrocław University of Science and Technology, Faculty of Chemistry, 7/9 Gdańskiego, 50-344, Wrocław, Poland



ARTICLE INFO

Keywords:
Long-chain *n*-alkanes
Hydroisomerization
Cold flow properties
AlSBA-15
BEA
MOR

ABSTRACT

In this study, the Pt (0.5 wt%) catalysts supported on the bimodal composite materials consisting of AlSBA-15 and zeolite (BEA or MOR) were used for hydroisomerization of the long-chain *n*-alkanes. Consideration was given to the method by which the AlSBA-15 and zeolite (20 wt% concentration) were combined: (i) by adding the zeolite to AlSBA-15 synthesis gel (*Method 1*) and (ii) by mechanical mixing the zeolite and AlSBA-15 powders (*Method 2*). The experiments of hydroisomerization of *n*-hexadecane were carried out using a fixed bed flow reactor system (5 MPa; 260–360 °C; WSHV, 3.5 h⁻¹; H₂:CH, 350:1 Nm³/m³). It was found that the synthesis of the supports according to *Method 1* resulted in a formation of new mesopores in the “zeolitic” phase of AlSBA-15 + zeolite, and also in a moderate acidity of these materials. The catalysts supported on the carriers prepared according to *Method 1* exhibited higher activity and isomerization selectivity than these supported on the carriers prepared according to *Method 2*. The *Method 1* yielded the Pt/AlSBA-15 + BEA catalyst displaying the highest isomerization selectivity (together with the highest contribution of monobranched isomers) and the lowest cracking selectivity.

1. Introduction

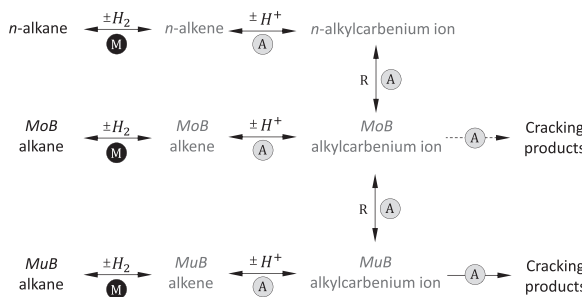
Hydroisomerization of the long-chain *n*-alkanes is an important process in the production of high-quality diesel fuels. It plays a significant role in the refining of crude oil fractions [1] but also in conversion of long-chain *n*-alkanes derived from alternative raw materials, *e.g.* from low-temperature Fischer-Tropsch (LTFT) conversion of (*bio*-)syngas [2–4] or hydrotreating of vegetable oils (HVO) [5,6]. The Biomass to Liquids (BtL) process involving the gasification of lignocellulose to (*bio*-)syngas followed by its conversion *via* LTFT reactions constitutes one of the most promising technologies for the production of high-quality second generation renewable diesel fuel [7,8]. The LTFT technology using (*bio*-)syngas is already operated on a small commercial scale by Linde Engineering Dresden [9]. Moreover, the hydroprocessing of triglycerides from plant oils (or optionally animal fats) into green paraffinic products has drawn much attention as a perfect method to produce *bio*-derived diesel fuel. There are few industrial licenses for the production of liquid hydrocarbon fractions by hydroconversion of triglycerides, among which the most well-known is the Honeywell UOP technology manufacturing Green Diesel® [10] and NesteOil Corporation process producing NExBTL Diesel® (NExGeneration Biomass-to-Liquid) [11]. Both the LTFT and HVO derived middle distillates are characterised by the absence of sulphur and aromatic compounds

whose presence in crude oil derived fuels leads to pollutants emissions. Furthermore, their paraffinic nature provides a high cetane number, but at the same time, it is the reason for unfavourable low-temperature properties that limits their direct application as the blending components for diesel fuel. The upgrading of the cold flow properties adjusted to the current requirements can be accomplished by the additional catalytic processing, *i.e.* catalytic hydroisomerization of *n*-alkanes to their branched derivatives. Compared to the *n*-alkanes, the *i*-alkanes with the same number of carbon atoms exhibit more favourable low-temperature properties (*i.e.* the *i*-alkanes display lower melting points than their straight-chain analogues). Among *i*-alkanes, the monobranched ones show not only the preferable low-temperature properties but also, they display cetane numbers almost as high as their linear counterparts. That makes them the most desirable diesel fuel components and in consequence, the most desirable hydroisomerization products [12,13].

The hydroisomerization of *n*-alkanes (**Scheme 1**) takes place over the bifunctional catalysts containing both the metal sites for dehydrogenation/hydrogenation and the Brønsted acid sites from the support for skeletal isomerization *via* carbenium ions [14]. According to the monomolecular isomerization mechanism, the *n*-alkanes are dehydrogenated on the metal sites and created this way the *n*-alkenes are protonated on the Brønsted acid sites to the corresponding transitional

* Corresponding author.

E-mail address: karolina.jaroszewska@pwr.edu.pl (K. Jaroszewska).



Scheme 1. Reaction network for hydroisomerization/hydrocracking of *n*-alkanes over bifunctional catalysts; M, metal sites; A, Brønsted acid sites; R, rearrangement of carbenium ions; MoB, monobranched; MuB, multibranched.

alkylcarbenium ions. Obtained secondary carbenium ions undergo rearrangement through the protonated cyclopropane (PCP) intermediates to the most stable tertiary carbenium ions. The monobranched carbocations are deprotonated over the acid sites to the branched alkenes, which are then hydrogenated over the metal sites to the corresponding monobranched isomers. Susceptibility of monosubstituted *i*-alkanes for cracking is low. However, if the acid sites are strong enough, the monobranched tertiary carbenium ions undergo further rearrangement to multibranched carbenium ions. The multisubstituted carbocations can either desorb from the catalyst surface as multibranched *i*-alkanes *via* deprotonation on the Brønsted sites followed by hydrogenation on metal or fall to cracking (β -scission). It is well known that the proper balance between metallic and acidic functions strongly affects the properties of a catalyst, especially its selectivity towards isomerization [15–17]. Dehydrogenation/hydrogenation properties of bifunctional catalysts are provided by the noble metals in mono- or bimetallic systems, usually Pt [18–20] and Pd [1,21], by the transition metal sulphides, *i.e.* Ni-W-S [22] or Ni-Mo-S [23] and by the multicomponent systems including both transition and noble metals, *e.g.* Ni-Pt-W [24] and Ni-Pd [25]. It has been showed that the noble metals containing catalysts display the best catalytic properties and show higher dehydrogenation/hydrogenation activity and higher selectivity towards isomers when compared to transition metals based catalysts [19]. The number of metal sites must be sufficient: (i) to supply a maximum of alkene intermediates to the acid centres, (ii) to hydrogenate rapidly the primary branched carbenium ions before further isomerization and finally (iii) to avoid the scission of C–C bond. If the dehydrogenation/hydrogenation function is strong enough, the pivotal influence on the activity and selectivity of the catalysts is exerted by the support, *i.e.* by their acidity and texture [26]. Thus, the modification of the physico-chemical properties of the supports is one of the preferred modes for performance improvement of the catalyst in a hydroisomerization process. Many attempts have been made to develop the isomerization catalysts through the selection of the proper carrier; nevertheless, they are mostly based on different kinds of silica-alumina supports, *e.g.* amorphous silica-aluminas [1,19], zeolites [21,27–29], silicoaluminophosphates [30] as well as mesoporous materials [31]. The most widely known group of supports are zeolites. Although the catalysts supported on zeolites show high activity and stability, they also exhibit a high cracking activity due to the presence of strong Brønsted acidic sites and/or the diffusion limitations promoting the cleavage of C–C bond [32]. To be more precise, their hydroconversion activity is very high, but often at the expense of the isomerization selectivity. Low isomerization selectivity is ascribed to the high number of acid sites encountered by the alkene intermediates during their diffusion between two Pt sites [33–35]. Along with the discovery of Al substituted ordered mesoporous materials such as AlMCM-41, AlSBA-15 or related mesoporous materials, the possibility of using carriers other than zeolites as the supports for advanced isomerization catalysts has appeared [36–40]. In these supports, the acidity and dimensions of the uniform system of channels can be tailored by selecting the Si/Al ratio and the

dimension of the template, respectively. Moreover, those materials contain the acidic OH groups of lower strength than the ones in zeolites. Moderate acidity favours the preferential formation of monobranched isomers, whereas high surface area provides high dispersion of the metallic phase what shortens the average distance between both types of catalytic centres. On the other hand, over the mesoporous materials supported catalysts with too low number of Brønsted acid centres, high catalytic activity is achieved at high reaction temperatures what may result in overcracking. It seems that the selective hydroisomerization is such a complex reaction that single component supports cannot efficiently meet all the requirements for catalytic performance such as high activity, unique isomerization selectivity and low activity in C–C bond cleavage.

The development of a new group of composite carriers, which are usually multicomponent solids, opens new possibilities for the enhancement of the activity of hydroisomerization catalyst [41]. The blending of two or more catalytic materials in a composite catalytic system usually either enables the average features or improves the functions of the main constituent due to a synergic effect between components. Taking into account the key role of the pore size and the acidity, it seems that composite materials with a hierarchical porous structure consisting of zeolite and ordered mesoporous material may be suitable supports for effective isomerization catalysts. The presence of zeolite (with crystalline structure and well-defined micropore system) increases the acidity (the number and strength of Brønsted acid site) and ensures high thermal stability. It can be expected that carrier acidity increase gives an increase in the catalytic activity [42] and enables the reaction to be carried out at lower operating temperatures [43]. On the other hand, the incorporation of mesoporous material into the hierarchical catalyst facilitates the diffusion of the long-chain hydrocarbons and therefore, it reduces the residence time of products in pores what minimises the occurrence of secondary reactions such as cracking. Thus, composite hierarchical materials combine the advantages of zeolites *via* providing high activity, and mesoporous materials *via* elimination of diffusion limitations what consequently enables high selectivity to isomers. The Pt catalysts supported on micro-mesoporous composite carriers have only been used to a limited extent for the hydroisomerization of *n*-alkanes [41,44,45].

In keeping with the foregoing, it is interesting to study the catalytic behaviour of the Pt (0.5 wt%) catalysts based on the AlSBA-15 + zeolite composite supports in hydroisomerization of the long-chain *n*-alkanes. In this work consideration was given to: (i) the effect of zeolite addition to the AlSBA-15, (ii) the effect of the method of composite catalyst preparation as well as (iii) the effect of the type of introduced zeolite. The properties of the AlSBA-15 materials were modified with zeolite (BEA or MOR) using two methods: by adding the zeolite in the AlSBA-15 synthesis step (*Method 1*) and by physical combining both the zeolite and AlSBA-15 powders at the carrier shaping stage (*Method 2*).

2. Experimental

2.1. Catalyst preparation

2.1.1. Synthesis of AlSBA-15

AlSBA-15 material with Si/Al ratio of 7 was synthesized following the procedure reported by Vinu et al. [46]. 4.0 g of micellar matrix *i.e.* Pluronic P123 ($\text{EO}_{20}\text{PO}_{70}\text{EO}_{20}$, Aldrich) was dissolved in 30 ml of distilled water and stirred for 2 h. Subsequently, 70 ml of 0.28 M HCl was added and it was mixed until it became homogenous solution (for about 2 h). Then, 8.5 g of tetraethyl orthosilicate (TEOS, Aldrich) was added along with 1.2 g of aluminium isopropoxide ($[(\text{CH}_3)_2\text{CHO}]_3\text{Al}$, Aldrich) and the obtained mixture was then stirred for 24 h at 40 °C. Next, the synthesis gel (with the molar composition of 1TEOS:0.12Al₂O₃:0.016P123:0.50HCl:136H₂O) was transferred to PTFE bottle and heated at 120 °C for 24 h under static conditions. The resulting solid material was filtered and washed with distilled water few times and

then dried for 12 h at 100 °C. The *as*-synthesized AlSBA-15 sample was calcined at 550 °C for 6–8 h to remove structure directing agent.

2.1.2. Synthesis of bimodal AlSBA-15 + zeolite supports (Method 1)

In the *Method 1* the supports were obtained by adding the H-form of zeolite BEA (CP811E, Zeolyst, Si/Al = 75) or MOR (CBV90A, Zeolyst, Si/Al = 45) during the preparation of AlSBA-15. The synthesis of AlSBA-15 was carried out following the procedure described in section 2.1.1, with the exception that after 24 h gel stirring at 40 °C the synthesis was stopped, and 20 wt% of zeolite (BEA or MOR) was added. The resulting mixture was stirred for a few minutes and then treated hydrothermally at 120 °C for 24 h in PTFE bottle. Solid products were filtered off and washed using deionised water until the neutral pH was obtained. The *as*-synthesized micro-mesoporous materials were first dried at 110 °C and next calcined at 550 °C for 6–8 h. The resulted carriers were denoted as SBA_BEAl(1) and SBA_MOR(1).

2.1.3. Synthesis of the bimodal AlSBA-15 + zeolite supports (Method 2)

The *Method 2* involved mechanical kneading of AlSBA-15 and zeolite powders. 20 wt% zeolite (BEA or MOR) was mixed with calcined AlSBA-15 prepared by the procedure described in section 2.1.1. The resulting supports were denoted as SBA_BEAl(2) and SBA_MOR(2).

2.1.4. Preparation of Pt catalyst

The AlSBA-15 powder and AlSBA-15 + zeolite materials were blended with 20 wt% of AlO(OH) (Pural 400, Sasol GmbH, after calcination γ -Al₂O₃) which was used as a binder. The obtained mixtures were peptised with 3% nitric acid (V) and then shaped into the cylindrical extrudates. The resulting pellets were dried for 12 h at 110 °C and then calcined at 450 °C for 6 h. The Pt catalysts were prepared via dry impregnation of already formed and calcined extrudates (0.40–0.63 mm in size) using hexachloroplatinic acid (H₂PtCl₆). In all the catalysts under the study the nominal Pt concentration was 0.5 wt%. The impregnated materials were dried (12 h at 110 °C) and calcined with gradual rise of temperature at the final temperature being 450 °C (3 h).

All of the supports and catalysts are listed in Table 1. The catalysts were denoted as: Pt/AlSBA-15 (AlSBA-15 supported catalyst), Pt/SBA_BEAl(1) and Pt/SBA_MOR(1) (the catalysts supported over AlSBA-

Table 1
Textural properties of the supports and the catalysts.

Sample	S_{BET} (m^2g^{-1})	V_T^a (cm^3g^{-1})	S_{MES}^b (m^2g^{-1})	V_{MES}^c (cm^3g^{-1})	d_{BJH}^d (nm)
AlSBA-15 ^b	788	1.23	634	1.09	7.7
AlSBA-15 ^b	616	1.19	555	0.81	7.7
Pt/AlSBA-15	579	0.99	442	0.75	7.9
<i>Supports and catalysts obtained by Method 1:</i>					
SBA_BEAl(1) ^b	736	1.12	613 (518) ^T	0.73	7.8
SBA_BEAl(1) ^b	541	0.91	312	0.55	7.7
Pt/SBA_BEAl(1)	524	0.93	302	0.51	7.7
SBA_MOR(1) ^b	694	1.23	584 (509) ^T	0.88	7.8
SBA_MOR(1) ^b	647	0.99	589	0.75	7.6
Pt/SBA_MOR(1)	452	0.80	353	0.58	6.5
<i>Supports and catalysts obtained by Method 2:</i>					
SBA_BEAl(2) ^b	529	1.00	217	0.42	7.6
Pt/SBA_BEAl(2)	485	0.88	220	0.44	7.8
SBA_MOR(2) ^b	492	0.72	392	0.52	5.5
Pt/SBA_MOR(2)	440	0.73	315	0.47	5.7

^aTheoretical S_{MES} values calculated on the basis of the S_{MES} values displayed by parent components and considering the proportion of the support components.
^bSupports shaped with binder.

^aTotal pore volume determined at $p/p_0 > 0.99$.

^bSurface and volume of mesopore from *t*-plot.

^cSurface and volume of mesopore from *t*-plot.

^dPore diameter (BJH method).

^pPowdered supports without binder.

15 + BEA and AlSBA-15 + MOR prepared by *Method 1*, respectively) as well as Pt/SBA_BEAl(2) and Pt/SBA_MOR(2) (the catalysts supported over AlSBA-15 + BEA and AlSBA-15 + MOR prepared by *Method 2*, respectively). It must be noticed, that Table 1 shows also the data for calcined powders (marked ^p) and supports extruded with the binder (marked ^b). For the clarity of the manuscript, the corresponding catalysts were not marked with ^b although they were prepared by using carriers shaped with a binder.

2.2. Catalyst characterisation

2.2.1. Texture

The textural properties were measured by the nitrogen adsorption at -196 °C, using a Autosorb-1C Quantachrome analyser. Prior to the adsorption measurements, the samples were degassed in vacuum at 150 °C for 6 h (analysis time 13 h). The total surface area of the samples was determined using the BET model. The distribution of pore sizes was calculated according to the Barrett-Joyner-Halenda method (BJH).

Powder XRD data were recorded in a X'Pert Pro equipment (PANalytical) with CuK α radiation (0.154 nm, 40 kV, 40 mA). Scanning was carried out with a 0.026° step and in range from 0.5 to 5° and from 10 to 80° 2 θ for mesoporous AlSBA-15 and zeolites, respectively.

2.2.2. Acidity

Acidity was determined using pyridine infrared spectroscopy (Py-IR). The IR spectra were registered using a Bruker Vector 22 spectrophotometer. The samples in the form of tablets were placed inside the FTIR quartz chamber and degassed under vacuum at 400 °C for 1 h. Next, the samples were saturated with pyridine at 150 °C and desorbed at 150, 200, 250, 300 and 350 °C in vacuum for 30 min. The IR spectra were registered in the 1400–1700 cm⁻¹ range. The quantitative calculation of Brønsted and Lewis acid sites was made with respect to the integrated area of IR vibrational bands observed at about 1545 cm⁻¹ and 1454 cm⁻¹, respectively.

2.2.3. Characterisation of the metal function

The Pt dispersion was determined by the H₂ chemisorption using a Micromeritics ASAP 2020 apparatus. Before the H₂ chemisorption, each sample was reduced *in situ* at 450 °C for 1 h in flowing of H₂. Next, the sample was degassed at the same temperature and cooled down to 35 °C under He flow. The H₂ chemisorption isotherms were determined within the pressure range from 10 to 450 Torr. The Pt dispersion was calculated at the chemisorption stoichiometry of H:Pt = 1.

2.2.4. TEM

The micro-mesoporous structure of the samples was investigated with a Philips CM-20 Super-Twin TEM microscope, operating at 160 kV and providing 0.25 nm resolution. The samples were dispersed in methanol and placed on the microscope copper grid covered with a carbon film.

2.2.5. SEM

Scanning electron microscopy (SEM) observations were carried out using Hitachi S-3400 N operating at 30 kV. Prior to analysis, the samples were sprayed with an approximately 100 nm thick carbon layer.

2.3. Catalytic experiments

The catalytic hydroisomerization of *n*-hexadecane (*n*-C₁₆) was carried out in a high-pressure stainless-steel flow fixed bed reactor (*i.d.* = 8 mm). In each run the reactor was charged from bottom to top in five parts. The bottom was first loaded with a small piece of quartz wool and then with 1 cm³ of inert material (1.2 mm SiC). Next, the catalyst bed of approximately 80 mm long was packed with 3 cm³ of catalyst (0.40–0.63 mm) diluted with 1 cm³ of SiC. The top part of the reactor was loaded with SiC in an amount enabling to fill the remaining

empty space in the reactor, and finally, with a small piece of quartz wool. Reaction was performed under the hydrogen pressure of 5 MPa, the H₂:CH molar ratio of 4.6, the WHSV of 3.5 h⁻¹ and at the temperature range of 280–340 °C. Before the activity test, the catalyst was reduced at 450 °C under 5 MPa hydrogen pressure for 3 h. The liquid samples were collected at 3.5 h intervals and analysed using the gas chromatography (Perkin Elmer Clarus 580) with Elite 1 column (60m × 0.53mm × 1.5 µm).

The liquid reaction products have been grouped as follows:

- (i) *i*-C₁₆ (hydroisomerization products), including MoBG₁₆ (mono-branched isomers), DiBG₁₆ (dibranched isomers) and MuBG₁₆ (multibranched isomers),
- (ii) C₃–C₁₃ (hydrocracking products),
- (iii) CB (carbon mass balance, *i.e.* low-molecular-weight compounds and tar).

Hydrocarbons with 14 and 15 carbon atoms (produced in hydrogenolysis of *n*-C₁₆) were detected only in the case of Pt/AlSBA-15 catalyst (0.2 wt%).

3. Results and discussion

3.1. Texture of the AlSBA-15 material and the Pt/AlSBA-15 catalyst

Fig. 1 shows the low-temperature nitrogen adsorption-desorption isotherms and pore size distributions of AlSBA-15 material, shaped with binder AlSBA-15 support and Pt/AlSBA-15 catalyst. According to the IUPAC classification, the isotherm of AlSBA-15 is of type IV (Fig. 1Aa) with capillary condensation step around p/p_0 of 0.75, what is characteristic for mesoporous molecular sieves. Furthermore, a H1-type hysteresis loop was observed, which is typical for regular mesoporous structures with double-opened cylindrical-shape pores. The highly ordered mesoporous structure of AlSBA-15 is also confirmed by a low-angle XRD presented in Fig. 1B. Intense diffraction peaks at 2θ around 0.9, 1.6 and 1.8° indexed as (1 0 0), (1 1 0) and (2 0 0) planes are associated with the *P6mm* hexagonal symmetry typical for the SBA-15 material [47]. The presence of a hexagonal and regular array of uniform

channels is also corroborated by TEM (Fig. 1C).

The extrusion procedure of AlSBA-15 with 20 wt% of binder followed by impregnation with H₂PtCl₆ (Pt/AlSBA-15 catalyst) does not alter the characteristic shape of nitrogen adsorption-desorption isotherm for mesoporous materials (Figs. 1Ab and 1Ac). However, presented results have revealed that application of the above procedure decreases the BET surface area (S_{BET}) by about 220 m² g⁻¹ and pore volume by 0.2 cm³ g⁻¹ as compared to the pure AlSBA-15 sample (Table 1).

3.2. Texture of the Pt/AlSBA-15 + zeolite composite catalysts

The low-temperature N₂ adsorption-desorption isotherms and the pore size distributions of the supports and Pt catalysts are plotted in Fig. 2. For all tested samples type of IV isotherm with characteristic H1 hysteresis loop is registered, what proves the presence of uniform and cylindrical mesopores in the powdered and shaped supports as well as in the Pt catalysts. However, there are some changes in the textural parameters of the AlSBA-15 + zeolite composite supports and the Pt catalysts in respect to the parent AlSBA-15 (Table 1). As can be expected, all of the composite materials (carriers and catalyst) show lower S_{BET} in comparison with the AlSBA-15 sample, what is a result of preparation procedure involving the zeolite incorporation, shaping with a binder and Pt deposition. The composite materials prepared with *Method 1* show higher S_{BET} than those obtained with *Method 2* (Table 1) regardless of the introduced zeolite. The comparison of structural parameters has also revealed that the carriers (and consequently the catalysts) obtained by the addition of BEA zeolite to AlSBA-15 display higher S_{BET} than those prepared with MOR zeolite.

A clear indication for a presence of ordered hexagonal structure in the investigated catalysts is provided by the low-angle XRD patterns (Fig. 3). There are visible three reflections at 2θ = 0.98, 1.6 and 1.8° corresponding respectively to (1 0 0), (1 1 0) and (2 0 0) planes in the hexagonal structure of SBA-15.

It is also worth noting that in the bimodal supports, the crystalline structure of zeolite is preserved regardless of the synthesis method and the zeolite type that was introduced. The wide-angle XRD patterns of BEA containing samples (Fig. 4A) show diffraction signals at *ca.* 12–14°

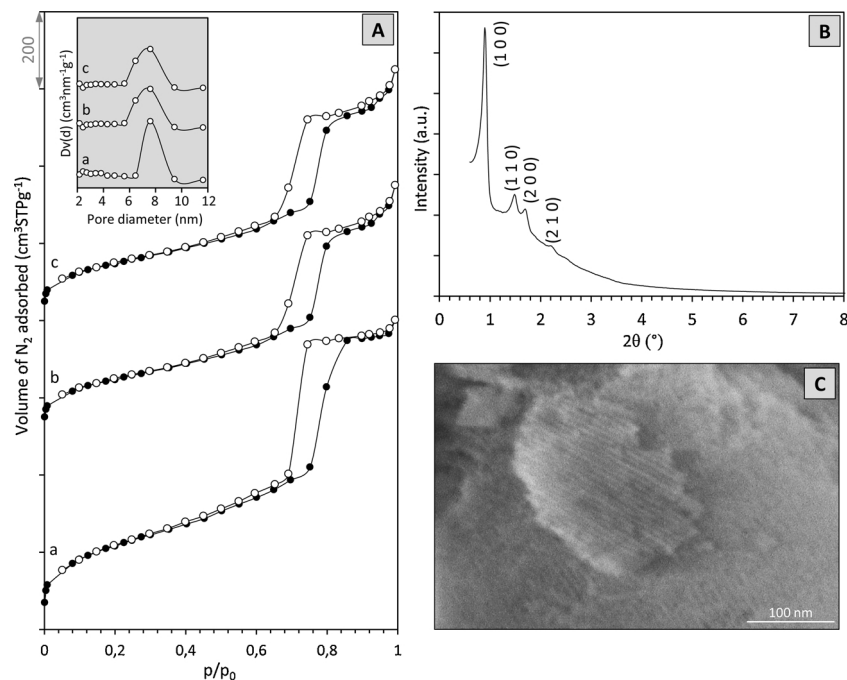


Fig. 1. Characterization of supports and catalysts; A) low-temperature N₂ adsorption-desorption isotherms and pore size distributions of a) powdered AlSBA-15P, b) extruded AlSBA-15B and c) Pt/AlSBA-15 catalyst; B) low-angle XRD pattern and C) TEM image of AlSBA-15P.

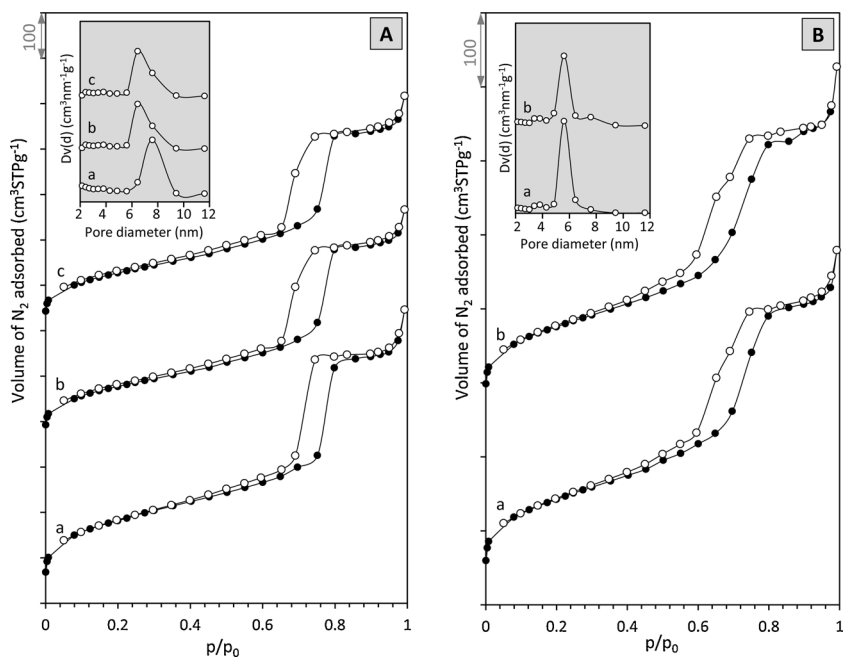


Fig. 2. Low-temperature N₂ adsorption-desorption isotherms and the pore size distributions of AlSBA15 + BEA carriers and Pt catalysts; **A**) synthesized according to *Method 1*: a) SBA_BEAlP (powder), b) SBA_BEAlB (extruded with binder) and c) Pt/SBA_BEAl; **B**) synthesized according to *Method 2*: a) SBA_BEAl2B (extruded with binder) and b) Pt/SBA_BEAl2.

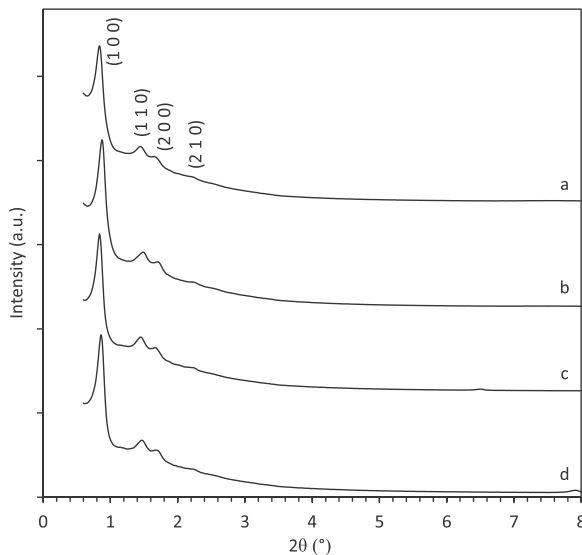


Fig. 3. Low-angle XRD patterns of: a) Pt/SBA_BEAl, b) Pt/SBA_MOR(1), c) Pt/SBA_BEAl2 and d) Pt/SBA_MOR(2).

and 22.5° that according to JCPDS 48-0074 are characteristic for BEA [48]. Also, the diffractograms of MOR containing samples (Fig. 4B) match well with JCPDS database for MOR phase (according to JCPDS 43-0171 lines at 2θ around 9–14°, 22–27°) [49]. The XRD spectra do not show any evidence of either extra lattice crystalline compounds or long-range amorphisation of the zeolite. Nevertheless, the intensity of reflexions typical for the zeolite in the bimodal materials is lower compared to pure BEA or MOR due to the presence of only 20 wt% of zeolite in the former case.

It is essential to confirm the structure of both the AlSBA-15 and zeolite when the catalysts are obtained *via Method 1* because this method involves SBA-15 phase crystallisation in the presence of zeolite particles and at the same time the contact of zeolite with the acidic environment. The stability of both AlSBA-15 and zeolite framework is also substantiated by the microscopy investigations. The representative SEM micrograph of Pt/SBA_BEAl (Fig. 5A) shows that the particles of AlSBA-15 are mainly spherically-shaped. The surface of AlSBA-15

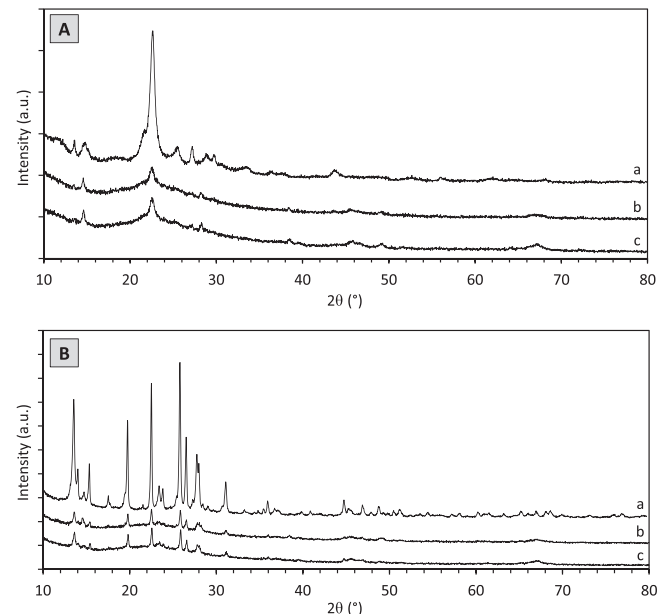


Fig. 4. Wide-angle XRD patterns collected for: **A**) BEA containing samples; a) BEA zeolite, b) Pt/SBA_BEAl and c) Pt/SBA_BEAl2 as well as for **B**) MOR containing samples; a) MOR zeolite, b) Pt/SBA_MOR(1) and c) Pt/SBA_MOR(2).

particles is partly covered with the zeolite crystals and the amorphous binder species. TEM image of Pt/SBA_BEAl catalyst (Fig. 5B) demonstrates an uniform and hexagonally ordered SBA-15-type mesostructure (some domains of amorphous material are attributed to the binder). Moreover, the crystals of BEA zeolite are clearly visible in the given TEM image (Fig. 5C). However, it should be pointed out that some mesopores are randomly distributed over the BEA crystals.

The phenomenon of the mesopores formation in BEA and MOR zeolite structure after adding the zeolite to AlSBA-15 synthesis gel (*Method 1*) has been supported by the textural parameters (Table 1). Since we investigate the catalysts which are multicomponent solids, it is difficult to directly verify the effect of formation of mesopores in the “zeolitic” part of the carrier after the analysis of the sorption data collected for the catalysts. Therefore, we decided to compare the

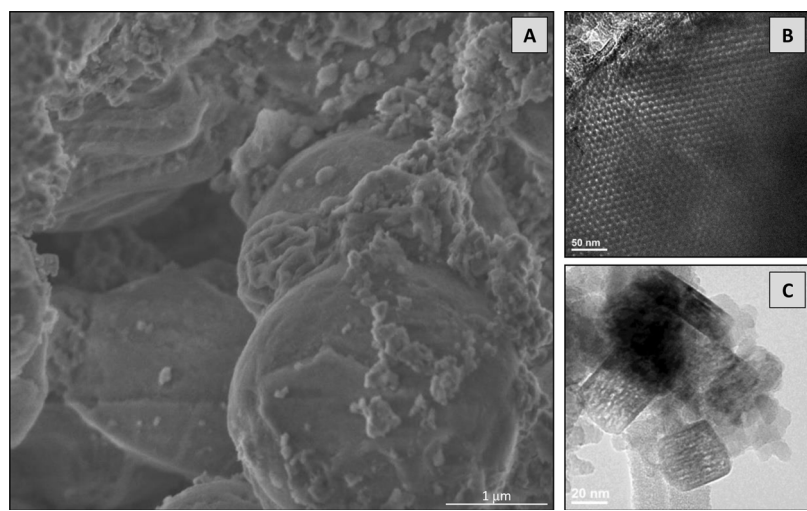


Fig. 5. Morphology of Pt/SBA_BEA(1) catalyst: A) SEM micrograph, B) TEM image of AlSBA-15 phase and C) TEM image of BEA zeolite crystals with mesopores.

differences in the mesopore surface (S_{MES}) of bimodal samples which are not formed with the binder (in Table 1 they are denoted SBA_BEA(1)^P and SBA_MOR(1)^P) with the values of theoretical S_{MES} . The theoretical S_{MES} value is calculated considering the S_{MES} values of parent components (*i.e.*, AlSBA-15, BEA and MOR) and their contribution as if the two-component carrier was a physical mixture. The BEA and MOR zeolites display the S_{MES} of approximately 52 and $8.2 \text{ m}^2 \text{ g}^{-1}$, respectively, while the AlSBA-15 displays S_{MES} of $634 \text{ m}^2 \text{ g}^{-1}$. Thus, the theoretical S_{MES} value calculated for mixtures of AlSBA-15 + BEA and AlSBA-15 + MOR amounts to 518 and $509 \text{ m}^2 \text{ g}^{-1}$, respectively. As can be seen, regardless of the zeolite used, the measured S_{MES} values are higher than the theoretical ones. Therefore, the calculations indicate that combining AlSBA-15 and zeolite *via* the addition of the zeolite to AlSBA-15 synthesis gel leads to the formation of new mesopores, *i.e.* the mesopores in the “zeolitic” part of the AlSBA-15 + zeolite samples. We believe that partial removal of Al atoms from the zeolite lattice takes place under the use of HCl solution in the synthesis of the AlSBA-15 + zeolite, what explains the generation of some mesopores within BEA and MOR crystals. Considering the structure of BEA and MOR zeolites, the BEA zeolite is more susceptible to dealumination [50]. However, it seems that under conditions used in our experiments, also MOR undergoes Al leaching to a large extent. Efficiency of Al removal is also strongly influenced by the Si/Al ratio within the zeolite framework, and the materials with lower Si/Al ratio are more prone to dealumination. In the present work, we have examined the MOR zeolite displaying a higher amount of Al atoms than BEA one (Si/Al ratio amounts to 45 and 75, respectively). Besides, it is well known that the consequence of dealumination is a decrease in the number of acid sites and the concomitant enhancement of the strength of acid centres. As is discussed later in the paper (section 3.4.), the catalyst whose bimodal carrier is obtained by incorporation of MOR zeolite into the AlSBA-15 synthesis gel (*i.e.* Pt/SBA_MOR(1)) exhibits the lowest number of Brønsted acid sites but of the highest strength. This seems to confirm the occurrence of dealumination within MOR crystals under the conditions of SBA_MOR(1) preparation procedure.

In principle, a typically controlled dealumination of zeolites is carried out for the purpose of acidity modification. Zeolite dealumination by acid leaching is also a commonly used technique for mesopore formation that yields the materials with hierarchical porous structure (*i.e.* mesoporous zeolites), but in consequence, it may lead to the lattice defects [51]. In order to create hierarchical structures with open and accessible mesopores, and to preserve the zeolite crystallinity, the dealumination may be combined with other techniques, *e.g.* the stabilisation of new-created mesopores by structure directing agents [52]. Local reorganisation of the zeolite structure which occurs around

the surfactant micelles accounts for the transformation of the initial zeolite mesopores into more uniform ones, so the final materials show high mesoporosity together with the lack of the zeolite crystallinity loss. It has been reported [53,54] that not all mesoporous materials and zeolites preserve structural arrangement and stability after catalysts preparation step, due to the different sensitivity to the treatments with chemical agents. In our work it was revealed that the destruction of “zeolitic” part in the composite of AlSBA-15 + zeolite materials obtained by *Method 1* is insignificant. Also, the mesoporous nature of AlSBA-15 phase is retained. To sum up, it can be concluded that some dual effect in the method of zeolite incorporation into the synthesis gel of AlSBA-15 accounts for the final structure of biporous materials. Firstly, the incorporation of zeolite into the AlSBA-15 synthesis gel involves the acid treatment, what leads to mesoporosity in BEA and MOR crystals. Secondly, the preservation of the zeolite structure may have resulted from stabilising role of Pluronic 123 that was introduced in order to create the AlSBA-15 phase.

Since the carriers obtained *via* *Method 2* consist of materials having defined structures before they were mixed, the detailed texture analysis of those materials is not crucial. Nevertheless one can observe that the supports obtained *via* *Method 2* display lower values of S_{MES} than the ones obtained *via* *Method 1*. However it should be taken into account, that the presented S_{MES} are measured for the composites (obtained by *Method 2*) which are the ternary mixtures (AlSBA-15, zeolite and binder), and the presence of the binder makes it difficult to provide a detailed discussion of the differences between measured S_{MES} and theoretical values.

3.3. Characterisation of the metal function

The wide-angle XRD spectra (Fig. 4) reveal no diffraction peaks corresponding to Pt containing phases in all of the investigated catalysts. It can be explained by the existence of highly dispersed, small Pt crystallites which are not detectable by XRD. It can also be caused by too low to be detected, the concentration of Pt phase (*i.e.* 0.5 wt%). Table 2 summarises the hydrogen chemisorption results (Pt dispersion, D ; Pt particle diameter, d_{Pt} ; Pt surface, S_{Pt}). The composition and preparation procedure of the supports only slightly affects the Pt dispersion. The Pt/AlSBA-15 catalyst displays the 57% Pt dispersion what corresponds to the presence of 2.0 nm sized Pt particles. Similarly, *Method 1* yields the catalysts with high Pt dispersion values. The Pt dispersion in BEA and MOR containing catalysts is 58 and 48%, and it corresponds to 2.0 and 2.3 nm Pt particles, respectively. Whereas *ca.* 44% Pt dispersion is noticed over the catalyst obtained with *Method 2*. Slightly lower Pt dispersion in those catalysts can be attributed to their

Table 2

Dispersion, Pt surface and particle size by chemisorption analysis of the catalysts.

Catalyst	D ^a (%)	S _{Pt} ^b (m ² g _{Pt} ⁻¹)	d _{Pt} ^c (nm)
Pt/AlSBA-15	57	142	2.0
Pt/SBA_BE(1)	58	144	2.0
Pt/SBA_MOR(1)	48	120	2.3
Pt/SBA_BE(2)	43	108	2.4
Pt/SBA_MOR(2)	44	109	2.6

^a Dispersion.

^b Pt surface area.

^c Average Pt particle diameter.

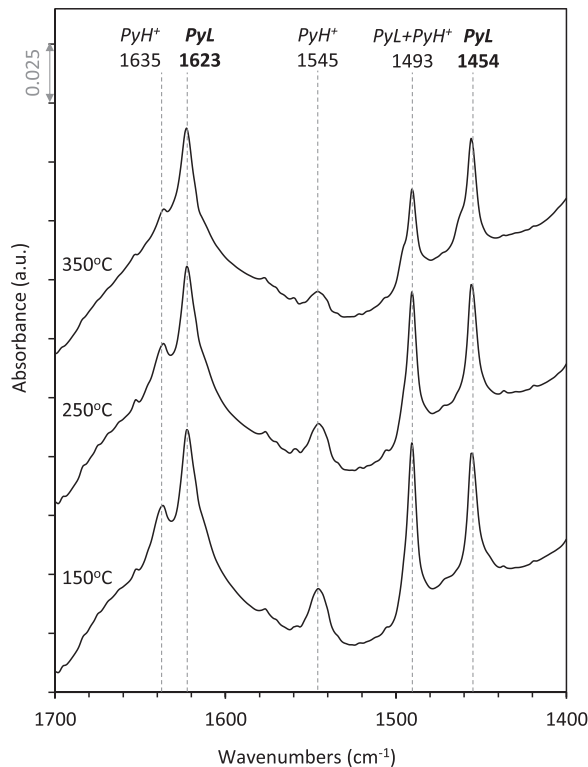


Fig. 6. FTIR spectra of pyridine adsorbed on Pt/SBA_BE(1) catalyst; PyH⁺, Brønsted acid sites; PyL, Lewis acid sites.

lower S_{BET}.

3.4. Acidity of the catalysts

The representative Py-IR spectra of Pt/SBA_BE(1) catalyst are shown in Fig. 6. The absorption bands at 1623 and 1454 cm⁻¹ are assigned to pyridine coordinated to the Lewis acid sites [55] and the bands at 1635 and 1545 cm⁻¹ are ascribed to pyridine bounded to the Brønsted acid sites [56]. Whereas the absorption band at 1493 cm⁻¹ corresponds to the vibrations of pyridine chemisorbed on both Lewis and Brønsted acid sites [57]. In general, in the investigated catalysts the Lewis acid sites may arise from the surfaces of the zeolite, AlSBA-15, γ-Al₂O₃ (a binder), as well as from Pt sites. In the case of the catalysts obtained with the *Method 1*, the Lewis acid sites might also be created during the supports preparation procedure, i.e. after the partial dealumination of the zeolite leading to the formation of the extraframework Al cations [58]. Whereas the presence of Brønsted acid sites is associated with the acidity of zeolite and AlSBA-15 material. It is also possible that the concentration of Brønsted acid sites may be improved by the residual chloride ions coming either from the decomposition of H₂PtCl₆ which was used as Pt precursor, or HCl which was used during the AlSBA-15 synthesis [59,60].

Table 3 lists the distribution of the acid sites for each catalyst. It is observed that the method of carriers preparation strongly influences the total acidity of the catalysts. When the AlSBA-15 + zeolite carriers are obtained in accordance with *Method 1*, the total acidity of the catalysts (ranging from 131 to 145 μmol_{Py}g_{cat}⁻¹) is slightly lower or comparable to the acidity of Pt/AlSBA-15 sample (146 μmol_{Py}g_{cat}⁻¹). Whereas when the carriers are prepared by *Method 2*, the total concentration of the acid sites is noticeably higher (211 – 215 μmol_{Py}g_{cat}⁻¹) than that displayed by Pt/AlSBA-15 sample. The total acidity of Pt/AlSBA-15 catalyst is attributed to the higher concentration of Lewis rather than Brønsted acid sites (comparison of total Lewis and Brønsted acid sites concentration i.e. measured at 150 °C). Contrary to that, in most AlSBA-15 + zeolite containing catalysts, Brønsted acidity is higher than Lewis acidity; only the Pt/SBA_MOR(1) (obtained by *Method 1*) exhibits a comparable amount of both types of acid centres.

Since the n-alkanes hydroisomerization involves the Brønsted acid centres, the detailed discussion of acidity changes upon the AlSBA-15 modification with zeolite is addressed to the sites being proton donors. As was expected, the presence of zeolite in the Pt/AlSBA-15 + zeolite catalysts results in higher concentration and strength of the Brønsted acidic sites (A₃₅₀/A₁₅₀) when compared with the Pt/AlSBA-15. It was found that the preparation procedure of the Pt/AlSBA-15 + zeolite catalysts has a noticeable effect on Brønsted acidity. The incorporation of BEA or MOR zeolite in accordance to *Method 1* gives the catalysts with 1.5 and 1.1-fold higher concentration of Brønsted acid sites than Pt/AlSBA-15 catalyst, (Brønsted acidity increased from 57 to 86 and 64 μmol_{Py}g_{cat}⁻¹, respectively). Although the modification of AlSBA-15 with MOR brings a smaller increase in the concentration of acid centres,

Table 3

Acidity of Pt catalysts by Py-IR (μmol_{Py}g_{cat}⁻¹).

Catalyst	PyH ⁺ ^a						PyL ^b						
	150 °C	200 °C	250 °C	300 °C	350 °C	A ₃₅₀ /A ₁₅₀ ^d	150 °C	200 °C	250 °C	300 °C	350 °C	A ₃₅₀ /A ₁₅₀ ^d	PyH ⁺ + PyL ^c
Pt/AlSBA-15	57	50	29	21	7	0.12	89	78	78	70	67	0.75	146
Pt/SBA_BE(1)	86	64	43	29	14	0.16	59	53	51	49	48	0.81	145
Pt/SBA_MOR(1)	64	64	43	36	29	0.45	67	65	61	55	53	0.79	131
Pt/SBA_BE(2)	114	93	64	50	36	0.32	101	91	91	84	80	0.79	215
Pt/SBA_MOR(2)	114	93	71	50	29	0.25	97	91	86	82	76	0.78	211

^a Brønsted acid sites.

^b Lewis acid sites.

^c Total acidity defined as the concentration of pyridine molecules retained on both Brønsted and Lewis acid sites after outgassing at 150 °C.

^d The strength of the acid sites calculated as ratio of relevant peaks intensities.

there is a distinct rise in their strength. Among all examined samples, the Pt/SBA_MOR(1) exhibits the strongest Brønsted acid sites. The enhancement of the acidity is also observed in the case of the catalysts supported on carriers obtained with *Method 2*. The incorporation of a zeolite, irrespectively of the zeolite type, brings 2-fold increase in the concentration of Brønsted acid sites as compared to Pt/AlSBA-15 catalyst (Brønsted acidity increased from 57 to 114 $\mu\text{mol}_{\text{Py}}\text{g}_{\text{cat}}^{-1}$). Doping the AlSBA-15 with both types of zeolites leads to more than 2-fold increase in the strength of the sites. It is also observed that the concentration of Brønsted acid sites in the catalysts containing supports prepared by the combining the powdered components (*Method 2*) is higher than in their analogues prepared by *Method 1*.

In general, it seems that in spite of the fact that the applied BEA and MOR zeolites differ in Si/Al ratio and the structure (in consequence they vary in Brønsted acidity), the concentration of Brønsted acid sites in the final composite catalysts is not affected by the type of the zeolite but it is affected by the carrier preparation procedure. It can be caused by the fact that the acid sites located on the external surface of the zeolites are available to a greater extent in composites prepared by *Method 2* than in those obtained by *Method 1*. When the AlSBA-15 + zeolite supports are synthesized by addition of zeolite to AlSBA-15 synthesis gel (*Method 1*), the Brønsted acid sites of zeolite can partly be covered by the generated layer of AlSBA-15 phase [61].

3.5. Catalytic activity

The results of the catalytic tests of *n*-C₁₆ hydroconversion are presented in Table 4. As can be seen, the composition of the carrier and the method of zeolite incorporation into the support substantially influences the *n*-C₁₆ conversion. The catalysts containing zeolite exhibit higher catalytic activity than this based on AlSBA-15 alone; *i.e.* to obtain the comparable values of the conversion a lower temperature by about 40 °C is needed when use is made of bimodal catalysts as compared to AlSBA-15 supported one. With the Pt/AlSBA-15 catalyst, T_R range of 280–360 °C provides *n*-C₁₆ conversion of 7–90% while with the both BEA containing catalysts the temperature range of 280–320 °C

provides *n*-C₁₆ conversion of about 40–96%. When use is made of the Pt catalysts based over MOR containing carriers the conversion depends on the preparation method. And so, on Pt/SBA_MOR(1) the conversion is in the range of 17–95% (at 280–340 °C) while on Pt/SBA_MOR(2) it is in the range of 44–92% (at 280–320 °C). In the case of zeolite containing catalysts, the activity enhancement and the shift of the activity maximum towards lower T_R (as compared to Pt/AlSBA-15) is due to increased Brønsted acidity upon the modification of AlSBA-15 with zeolite. Furthermore, in the case of the catalysts prepared by *Method 1*, only a slight increase in Brønsted acidity is concomitant with a notable enhancement of *n*-C₁₆ conversion.

For all investigated catalysts, the *n*-C₁₆ conversion mostly leads to the formation of hydroisomerization and hydrocracking products (Table 4). In general, the yield of monobranched products (MoBC₁₆) drops with an increase in T_R. The low yield of MoBC₁₆ derivatives is accompanied by the greater yield of multibranched products (MuBC₁₆), and consequently higher yield of C₃ + C₁₃ products. Thus, the examined catalysts follow the classical mechanism of alkane hydroconversion in which alkene intermediates undergo successive isomerization steps before cracking.

The products distribution (Table 4) shows that for all tested catalysts the yield of *i*-C₁₆ passes through the maximum as the T_R increases. The maximal yield of isomers on Pt/AlSBA-15 catalyst (amounting to 51 wt%) is obtained at 77% of total *n*-C₁₆ conversion (at 340 °C). It can be observed that the highest *i*-C₁₆ yield on the BEA containing catalysts is achieved at comparable conversion value of 84% and on Pt/SBA_BE(1) and Pt/SBA_BE(2) catalysts it amounts to ca. 60 and 54 wt%, respectively. When use is made of MOR containing catalysts, the maximal *i*-C₁₆ yield is comparable with one for Pt/AlSBA-15 and it amounts to 53 wt% (at 91% conversion) on Pt/SBA_MOR(1) and 54 wt% (at 80% conversion) on Pt/SBA_MOR(2). Regardless of the preparation method of bimodal catalysts, in most cases, the maximal yield of *i*-C₁₆ isomers is registered at 300 °C (except for Pt/SBA_MOR(1) where it is reached at 320 °C). A significant issue is also the catalyst performance in hydroisomerization of *n*-alkanes in a view of MoBC₁₆ isomers yield. On Pt/AlSBA-15 catalyst, the maximal yield of the most desired *i*-

Table 4
Activity of the catalysts.

Catalyst	T _R (°C)	Conv. (%)	Hydroisomerization				Hydrocracking			CB ^e (wt%)	
			Yield (wt%)			Selectivity (%)	Yield (wt%)	Selectivity (%)			
			total <i>i</i> -C ₁₆	MoBC ₁₆ ^a	DiBC ₁₆ ^b		total <i>i</i> -C ₁₆	C ₃ + C ₁₃	<i>i</i> / <i>n</i> ^d (mol/mol)		
Pt/AlSBA-15	280	7.0	4.4	3.2	0.9	0.3	62.9	0.5	—	7.1	2.1
	300	16.2	11.5	8.2	2.4	0.9	71.0	2.5	—	15.4	2.2
	320	39.0	29.8	18.6	8.6	2.6	76.4	7.0	—	17.9	2.2
	340	76.6	51.1	18.6	13.8	16.6	66.7	23.4	2.6	30.5	2.1
	360	90.2	28.2	7.3	11.6	9.3	31.3	59.9	2.6	66.4	2.1
Pt/SBA_BE(1)	280	41.7	37.1	22.3	13.2	1.6	89.0	2.4	—	5.8	2.2
	300	83.9	59.5	15.9	25.0	18.6	70.9	22.3	3.9	26.6	2.1
	320	96.6	45.6	8.4	17.4	19.8	47.2	48.8	3.0	50.5	2.2
Pt/SBA_MOR(1)	280	16.8	12.8	10.0	2.0	0.7	76.2	1.9	—	11.3	2.1
	300	43.4	35.2	20.3	10.9	4.1	81.1	6.1	—	14.1	2.1
	320	90.9	52.8	15.6	20.6	16.6	58.1	36.0	4.8	39.6	2.1
Pt/SBA_BE(2)	280	44.9	29.3	6.5	12.8	10.0	30.9	63.2	4.4	66.6	2.4
	300	43.1	32.9	16.9	10.9	5.1	76.3	8.1	—	18.8	2.1
	320	82.7	54.3	15.9	22.6	15.7	65.7	26.4	4.2	31.9	2.0
Pt/SBA_MOR(2)	280	96.4	14.4	4.4	5.5	4.5	14.9	80.0	3.5	83.0	2.0
	300	44.2	32.3	18.3	10.0	4.0	73.1	9.7	—	21.9	2.2
	320	79.9	53.6	17.3	21.9	14.4	67.1	24.2	4.8	30.3	2.1
											2.3

^a MoBC₁₆, Mono-branched hexadecane isomers.

^b DiBC₁₆, Di-branched hexadecane isomers.

^c MuBC₁₆, Multi-branched hexadecane isomers.

^d *i*/*n* within C₃ + C₁₃ (mol/mol).

^e CB, Carbon mass balance.

alkanes is achieved at 320 °C (18.6 wt%). When use is made of the catalysts containing BEA or MOR zeolites incorporated by *Method 1*, the higher MoBC₁₆ yield is reached, being 22.3 and 20.3 wt%, respectively. Besides, the maximal concentration of MoBC₁₆ is observed at lower T_R than in the case of Pt/AlSBA-15 catalyst. The support preparation *via Method 2* leads to a slightly lower yield of MoBC₁₆ as compared to that achieved on Pt/AlSBA-15 (for Pt/SBA_BEA(2) and Pt/SBA_MOR(2) it equals 16.9 and 18.3 wt%, respectively). Among all isomers with more than one methyl group, dibranched isomers (DiBC₁₆) are also valuable fuels components since they exhibit higher cetane numbers than MuBC₁₆ ones and display excellent low-temperature properties. Therefore, it is also worth noting that regardless of the support composition and T_R, the DiBC₁₆ predominate among all the isomers with more than one methyl group.

The yield of C₃–C₁₃ fraction over Pt/AlSBA-15 catalyst falls within the range of 0.5–59.9 wt%. As presented in Table 4, the Pt/SBA_BEA(1) shows the lowest yield of hydrocracking products (about 2.4–48.8 wt% in the entire range of T_R) among all tested biporous catalysts. The yield of C₃–C₁₃ products on Pt/SBA_MOR(1), which is slightly less active than the former one (*i.e.* it works at somewhat higher T_R), varies between 1.9 and 63.2 wt%. One can observe that regardless of the zeolite type, the yield of the cracking products is comparable on both catalytic systems prepared in accordance to *Method 2*. And it is amounted to 8.1 – 80 and 9.7 – 75 wt% on Pt/SBA_BEA(2) and Pt/SBA_MOR(2), respectively.

The above presented measurements of catalytic activity show that the composition of the carries, as well as the method of their preparation, exerts an evident impact on the catalyst selectivity. It is well known that the catalysts with a high hydrogenation activity and a moderate acidity are usually more favourable for hydroisomerization than for hydrocracking. Also, the proper balance and proximity between the metal and acid sites (allowing the reaction over the acid sites to be the limiting step) has a pivotal influence on the selectivity of the hydroisomerization catalyst [62]. On the other hand, the activity and selectivity of the bifunctional catalyst depends on the character of its metal and acid functions, as well as on their balance, but only if there are no diffusion limitations [63]. In the case when the catalyst contains microporous material (*e.g.* zeolite), the catalytic performance is influenced by the geometry and dimensionality of the zeolite channels. Thus, considering the relatively high Pt dispersion in all studied catalysts, their activity may be looked at in the context of differences in their acidity and porous structure, that are resulting from the composition of the supports and applied preparation method.

With the Pt/AlSBA-15 catalyst (the case without diffusion limitations) the low activity and hydroisomerization selectivity may be linked with a relatively low number of Brønsted acid sites on its surface. The acidity provided by the AlSBA-15 carrier makes the catalyst active at high T_R what may promote cracking reactions. It is observed that the selectivity of the catalysts supported on carriers prepared by *Method 1* is very sensitive to the type of zeolite that was used. The results reveal that the Pt/SBA_BEA(1) provides the highest yield of isomers (with the highest MoBC₁₆ contribution) and the lowest yield of cracking products. Moreover, it is active at a lower T_R compared to the Pt/AlSBA-15 catalyst. We believe that the best catalytic performance of Pt/SBA_BEA(1) is explained by not only moderate acidity and sufficient Pt distribution guaranteeing the appropriate metal/acidity balance but also by the presence of secondary mesopores within BEA zeolite. It may be concluded that the enhanced activity of Pt/SBA_BEA(1) catalytic system is not affecting the hydroisomerization selectivity if the required metal/acidity balance is retained and the diffusion limitations are eliminated. As was presented earlier in the paper, there is a significant decrease in the selectivity to isomers, which is accompanied by the increase in the cracking selectivity after using the Pt/SBA_MOR(1). It appears that the low yield of isomers is obtained because the generation of secondary mesopores in MOR zeolite simultaneously leads to too strong Brønsted acid centres for efficient hydroisomerization.

When use is made of catalysts from *Method 2*, the highest concentration of Brønsted acid centres makes the both Pt/SBA_BEA(2) and Pt/SBA_MOR(2) catalytic systems more active in C–C bond cleavage than in alkane branching. However, comparing the selectivity to i-C₁₆ isomers on the catalysts prepared according to *Method 2*, one can state that the catalyst containing BEA zeolite shows slightly better performance than the one with MOR. Since both catalysts supported on the carriers prepared by *Method 2* exhibit similar acidity and sites of comparable strength, the small differences in isomerization activity appear as being controlled directly by their pore architecture, more precisely by the porous structure of introduced BEA or MOR zeolite.

Moreover, it can be concluded that the method by which AlSBA-15 and BEA are combined affects the acidity and porous structure of the catalysts, but it also seems to influence the homogeneity of the components in the final carrier. On the Pt/SBA_BEA(1) the selectivity to isomerization products is much higher (and simultaneously much lower selectivity to cracking products) than on the Pt/SBA_BEA(2). Therefore, good homogenization of BEA zeolite crystals in AlSBA-15 + zeolite (obtained by *Method 1*) will result in proximity of cooperating metal and Brønsted acid sites, and this may account for high efficiency of the Pt/SBA_BEA(1) catalytic system. Such a phenomenon is not observed when the AlSBA-15 is modified with MOR zeolite. However, the catalyst prepared by *Method 1* displays low overall activity (it works at higher T_R); therefore, it is difficult to follow the variations in the selectivity.

It was found in this work that zeolite structure strongly influences the distribution of cracking products as well as the degree of branching (*i/n*) within this fraction. The distribution of the cracked product in terms of carbon number at the highest yield of hydrocracking products obtained on the composite catalysts is compared in Fig. 7. On the BEA containing catalysts (regardless of the carriers preparation method) the distribution of cracked products with respect to the number of carbon atoms is almost symmetrical with the maximum positioned at C₈ (Fig. 7a and b). Such a distribution of cracking products indicates the lack or very small extent of a secondary cracking. In contrary, the distribution patterns obtained on the MOR containing catalysts (Fig. 7c and d) are unsymmetrical with a plateau appearing in the C₅–C₈ range of carbon numbers. It indicates that secondary cracking of primary products occurs on these catalysts to a greater extent when compared to catalysts supported on AlSBA-15 + BEA. It is possible, that stronger adsorption of primary products in MOR channels (when compared to those prevailing in BEA) results in secondary cracking [64].

The C₃–C₁₃ fraction produced on all bimodal catalysts composes of *i*-alkanes rather than *n*-alkanes. The values of *i/n* ratio within the C₃–C₁₃ fraction obtained on AlSBA-15 + MOR supported catalysts (regardless of the synthesis method) are higher than the ones found on corresponding catalysts supported on AlSBA-15 + BEA. The contribution of different types of β -scission of carbocations explains the variation in the values of *i/n* ratio registered within cracking products obtained on the catalysts having a different composition concerning the zeolite type. According to the mechanism of *n*-alkanes hydroconversion, the β -scissions of alkylcarbenium ion are: (*i*) type A, where *tri*-branched carbocation undergoes the β -scission yielding two branched molecules, (*ii*) type B, where *di*- or *tri*-branched carbocation undergoes the β -scission resulting in one branched and one linear hydrocarbon, and (*iii*) type C, where *di*-branched carbocation undergoes the β -scission to two linear alkanes [65]. It seems that the concentration of the *tertiary* carbenium ions is higher when use is made of the AlSBA-15 + MOR supported catalysts. The *tertiary* carbenium ion is cracked by the A-type β -scission, providing two isomerized compounds what consequently results in higher content of branched isomers in the cracking products. In the case of AlSBA-15 + BEA supported catalysts, the values of the *i/n* ratio suggest that type B and C of β -scission occurs to some extent.

To summarise, all above results reveal that the Pt/SBA_BEA(1) exhibits the best catalytic performance in *n*-C₁₆ hydroisomerization. It provides the highest yield of isomers and simultaneously, the lowest

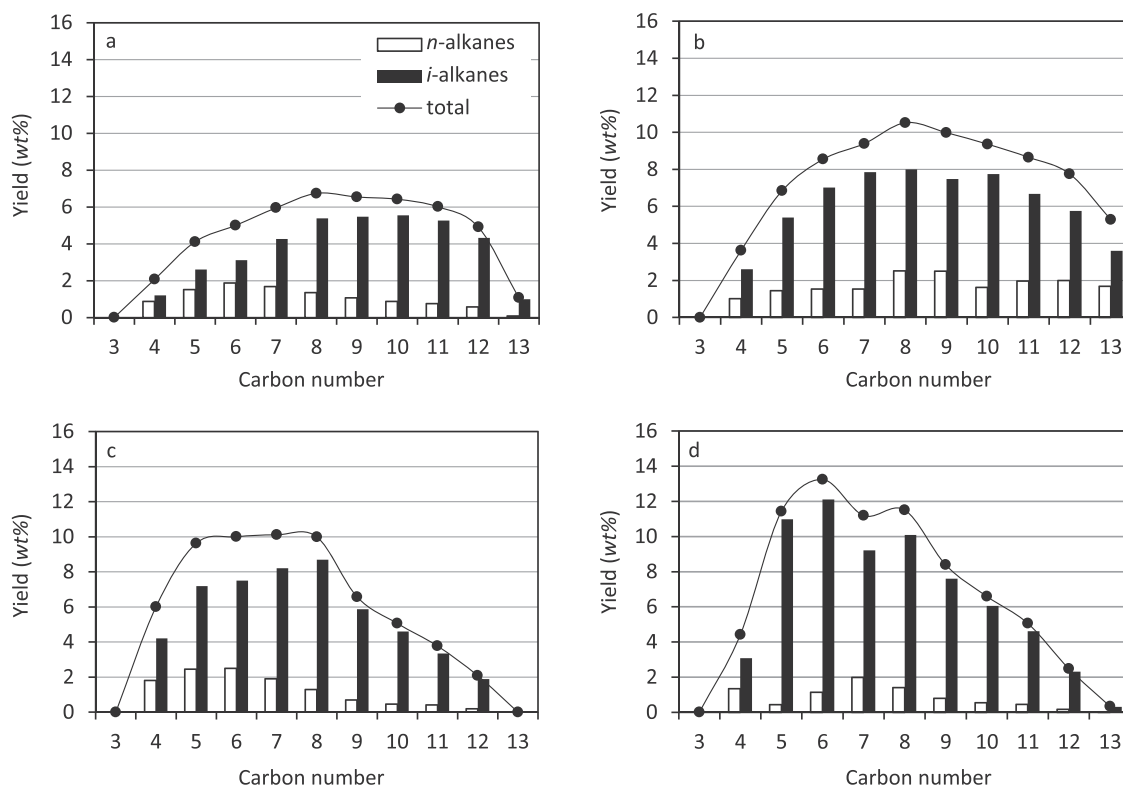


Fig. 7. Distribution of *n*-alkanes and *i*-alkanes by carbon number at a highest yield of hydrocracking products obtained over: a) Pt/SBA_BEAl, b) Pt/SBA_BEAt, c) Pt/SBA_MORl and d) Pt/SBA_MORt catalysts.

yield of cracking products. What is also important, it is active at lower T_R as compared to the Pt/AlSBA-15 catalyst. We believe that the best performance of Pt/SBA_BEAl is explained not only by its moderate acidity and sufficient Pt distribution but also by its features resulting from the method of carrier preparation used in this work. This includes a generation of extra mesopores in BEA zeolite that facilitates the mass transport and also good homogenization of the zeolite crystallites in a AlSBA-15 + BEA mixture, that provides a proximity of cooperating active sites. Although, further work is necessary to improve their performance, Pt/AlSBA-15 + BEA catalyst, due to its higher isomer selectivity, has a great potential to become a viable catalyst for hydroisomerization of long-chain *n*-alkanes.

4. Conclusions

The investigation has shown how the preparation method of bimodal supports of AlSBA-15 + zeolite designed for the advanced composite Pt (0.5 wt%) catalysts influences their catalytic performance in hydroisomerization of *n*-hexadecane. The properties of the AlSBA-15 were modified with 20 wt% of zeolite (BEA or MOR) using two methods: (i) by zeolite addition to the AlSBA-15 synthesis gel, which was followed by 24-hs hydrothermal treatment and extrusion of calcined materials with binder, and (ii) by physical mixing the zeolite and AlSBA-15 powders followed by the extrusion. On the basis of obtained the results the following conclusions have been drawn:

- 1 The addition of the zeolite to AlSBA-15 synthesis gel results in the formation of new mesopores, *i.e.* the mesopores in “zeolitic” part of the AlSBA-15 + zeolite bimodal samples. Leaching of aluminium atoms from the lattice of zeolite under the acidic conditions of AlSBA-15 phase crystallisation, explains the mesoporosity generation in BEA and MOR zeolite crystals.
- 2 The Pt catalysts supported on bimodal carriers consisted of AlSBA-15 and zeolite are more effective in *n*-hexadecane

hydroisomerization than the catalyst supported on AlSBA-15 alone. Low activity and low hydroisomerization selectivity of Pt/AlSBA15 is linked with relatively low number of Brønsted acid sites over its surface.

- 3 The Pt catalysts supported on the composites prepared by incorporation of zeolite into the AlSBA-15 synthesis gel display higher isomerization selectivity than their counterparts in which the supports were prepared by powders blending. It is especially pronounced when use is made of BEA containing carriers. A good homogenization of AlSBA-15 + zeolite mixtures may partly account for the efficiency of these catalytic systems by providing suitable proximity between metal and Brønsted acid sites.
- 4 The Pt catalyst supported on the AlSBA-15 + BEA carrier prepared *via* adding BEA into AlSBA-15 synthesis gel, displays the highest yield of isomers (together with the highest contribution of mono-branched ones) and the lowest yield of the cracking products. The applied preparation method makes it possible to obtain a Pt/AlSBA-15 + BEA catalyst with unique features, *i.e.* moderate acidity, proper proximity of cooperating active sites and also the presence of secondary mesopores within BEA zeolite.

Acknowledgements

The work was financed by a statutory activity subsidy from the Ministry of Science and Higher Education, Republic of Poland for the Faculty of Chemistry of Wrocław University of Science and Technology (0401/0144/18). We are grateful to Dr. Aleksandra Masalska from Wrocław University of Science and Technology for very helpful discussion of the results.

References

- [1] F. Regali, L.F. Liotta, A.M. Venezia, V. Montes, M. Boutonnet, S. Järas, *Catal. Today* 223 (2014) 87–96.
- [2] F.A.N. Fernandes, U.M. Teles, *Fuel Process. Technol.* 88 (2007) 207–214.

[3] F. Trippé, M. Frohling, F. Schultmann, R. Stahl, E. Henrich, A. Dalai, *Fuel Process. Technol.* 106 (2013) 577–586.

[4] C. Bouchy, G. Hastoy, E. Guillon, J.A. Martens, *Oil Gas Sci. Technol.* 64 (2009) 91–112.

[5] J.A. Martens, D. Verboekend, K. Thomas, G. Vanbutsele, J.P. Gilson, J. Pérez-Ramírez, *Chem. Sus. Chem.* 6 (2013) 421–425.

[6] C. Wang, Z. Tian, L. Wang, R. Xu, Q. Liu, W. Qu, H. Ma, B. Wang, *Chem. Sus. Chem.* 5 (2012) 1974–1983.

[7] S. Sartipi, M. Makkee, F. Kapteijn, J. Gascon, *Catal. Sci. Technol.* 4 (2014) 893–907.

[8] K.M. Cho, S. Park, J.G. Seo, M.H. Youn, S.H. Baeck, K.W. Jun, J.S. Chung, I.K. Song, *Appl. Catal. B Environ.* 83 (2008) 195–201.

[9] <http://www.linde-engineering.com>.

[10] A. Sonthalia, N. Kumar, *J. Energy Inst.* 92 (2019) 1–17.

[11] C. Kordulis, K. Bourikas, M. Gousi, E. Kordouli, A. Lycourghiotis, *Appl. Catal. B Environ.* 181 (2016) 156–196.

[12] R.C. Santana, P.T. Do, M. Santikunaporn, W.E. Alvarez, J.D. Taylor, E.L. Sughrue, D.E. Resasco, *Fuel* 85 (2006) 643–656.

[13] B. Creton, C. Dartiguelongue, T. Bruin, H. Toulhoat, *Energy Fuels* 24 (2010) 5396–5403.

[14] V.M. Akhmedov, S.H. Al-Khawair, *Catal. Rev.* 49 (2007) 33–139.

[15] H. Deldari, *Appl. Catal. A: Gen.* 293 (2005) 1–10.

[16] F. Alvarez, F.R. Ribeiro, G. Perot, C. Thomazeau, M. Guisnet, *J. Catal.* 162 (1996) 179–189.

[17] J. Weitkamp, *Chem. Cat. Chem.* 4 (2012) 292–306.

[18] Y. Liu, C. Liu, Z. Tian, L. Lin, *Energy Fuels* 18 (2004) 1266–1271.

[19] F. Regali, L.F. Liotta, A.M. Venezia, M. Boutonnet, S. Järas, *Appl. Catal. A: Gen.* 469 (2014) 328–339.

[20] Y. Wang, Z. Tao, B. Wu, J. Xu, Ch. Huo, K. Li, H. Chen, Y. Yang, Y. Li, *J. Catal.* 322 (2015) 1–13.

[21] F. Bauer, K. Ficht, M. Bertmer, W.D. Einicke, T. Kuchling, R. Gläser, *Catal. Sci. Technol.* 4 (2014) 4045–4054.

[22] Y. Rezgui, M. Guemini, *Appl. Catal.* 282 (2005) 45–53.

[23] K. Sakashita, T. Kimura, M. Yoshino, S. Asaoka, *J. Jpn. Petrol. Inst.* 54 (2011) 320–330.

[24] Y. Rezgui, M. Guemini, *Appl. Catal. A: Gen.* 374 (2010) 31–40.

[25] D. Karthikeyan, R. Atchudan, R. Sivakumar, *Chin. J. Catal.* 37 (2016) 1907–1917.

[26] S.V. Konnov, I.I. Ivanova, O.A. Ponomareva, V.I. Zaikovskii, *Microporous Mesoporous Mater.* 164 (2012) 222–231.

[27] S. Parmar, K.K. Pant, M. John, K. Kumar, S.M. Pai, *Energy Fuels* 29 (2015) 1066–1075.

[28] Y. Bi, G. Xia, W. Huang, H. Nie, *RSC Adv.* 5 (2015) 99201–99206.

[29] S. Mehta, B. Viswanathan, M. John, S. Pai, *J. Porous Mater.* 20 (2013) 1023–1029.

[30] S. Zang, S.L. Chen, P. Dong, G. Yuan, K. Xu, *Appl. Catal. A: Gen.* 332 (2007) 46–55.

[31] K. Fang, W. Wei, J. Ren, Y. Sun, *Catal. Lett.* 93 (2004) 235–242.

[32] R. Kenmogne, A. Finiels, C. Cammarano, V. Hulea, F. Fajula, *J. Catal.* 329 (2015) 348–354.

[33] F. Alvarez, F.R. Ribeiro, G. Perot, C. Thomazeau, M. Guisnet, *J. Catal.* 162 (1996) 179–189.

[34] N. Batalha, L. Pinard, C. Bouchy, E. Guillon, M. Guisnet, *J. Catal.* 307 (2013) 122–131.

[35] A. Astafan, Y. Pouilloux, J. Patarin, N. Bats, C. Bouchy, T.J. Daou, L. Pinard, *New J. Chem.* 40 (2016) 4335–4343.

[36] K. Sabyrov, N. Musselwhite, G. Melaet, G.A. Somorjai, *Catal. Sci. Technol.* 7 (2017) 1756–1765.

[37] P. Elangovan, C. Bischof, M. Hartmann, *Catal. Lett.* 80 (2002) 35–40.

[38] B.C. Gagea, Y. Lorgouilloux, Y. Altintas, P.A. Jacobs, J.A. Martens, *J. Catal.* 265 (2009) 99–108.

[39] X. Chen, M. Jia, G. Liu, X. Zhang, L. Wang, Z. Mi, *Appl. Surf. Sci.* 256 (2010) 5856–5861.

[40] S. Gong, N. Chen, S. Nakayama, E.W. Qian, *J. Mol. Catal. A: Chem.* 370 (2013) 14–21.

[41] P.T. Huyen, L.T.H. Nam, T.Q. Vinh, C. Martínez, V.I. Parvulescu, *Catal. Today* 306 (2018) 121–127.

[42] L. Wu, V. Degirmenci, P.C.M.M. Magusin, B.M. Szyja, E.J.M. Hensen, *Chem. Commun.* 48 (2012) 9492–9494.

[43] Y.G. Li, W.H. Xie, S. Yong, *Appl. Catal. A: Gen.* 150 (1997) 231–242.

[44] S.P. Elangovan, M. Hartmann, *J. Catal.* 217 (2003) 388–395.

[45] M. Zhang, C. Li, Y. Chen, C.W. Tsang, Q. Zhang, C. Liang, *Catal. Sci. Technol.* 6 (2016) 8016–8023.

[46] A. Vinu, V. Murugesan, W. Bohlmann, M. Hartmann, *J. Phys. Chem. B* 108 (2004) 11496–11505.

[47] G.M. Kumaran, S. Garg, K. Soni, M. Kumar, L.D. Sharma, G.M. Dhar, K.S.R. Rao, *Appl. Catal. A: Gen.* 305 (2006) 123–129.

[48] Q. Zhao, B. Chen, Z. Bai, L. Yu, M. Crocker, C. Shi, *Appl. Catal. B Environ.* 242 (2019) 161–170.

[49] K. Nakamoto, M. Ohshiro, T. Kobayashi, *J. Environ. Chem. Eng.* 5 (2017) 513–525.

[50] M.D. González, Y. Cesteros, P. Salagre, *Microporous Mesoporous Mater.* 144 (2011) 162–170.

[51] D. Verboekend, T.C. Keller, M. Milina, R. Hauert, J. Pérez-Ramírez, *Chem. Mater.* 25 (2013) 1947–1959.

[52] J. García-Martínez, M. Johnson, J. Valla, K. Li, J.Y. Ying, *Catal. Sci. Technol.* 2 (2012) 987–994.

[53] A. Rodríguez-Fernández, F.J. Llopis, C. Martínez, M. Moliner, A. Corma, *Microporous Mesoporous Mater.* 267 (2018) 35–42.

[54] A.A. Campos, C.R. Silva, M. Wallau, L.D. Dimitrov, E.A. Urquieta-González, *Stud. Surf. Sci. Catal.* 158 (2005) 573–580.

[55] W. Wu, E. Weitz, *Appl. Surf. Sci.* 316 (2014) 405–415.

[56] Y. Qiu, X. Hou, G. Liu, L. Wang, X. Zhang, *Microporous Mesoporous Mater.* 243 (2017) 176–185.

[57] H. Wei, K. Liu, S. Xie, W. Xin, X. Li, S. Liu, L. Xu, *J. Catal.* 307 (2013) 103–110.

[58] X. Lu, Y. Guo, C. Xu, R. Ma, X. Wang, N. Wang, Y. Fu, W. Zhu, *Catal. Commun.* 125 (2019) 21–25.

[59] B. Ozimek, J. Grzechowiak, B. Radomyski, G. Szezyglowska, *React. Kinet. Catal. Lett.* 17 (1981) 139–142.

[60] B.H. Shi, O.Y. Gutiérrez, H. Yang, N.D. Browning, G.L. Haller, J.A. Lercher, *ACS Catal.* 3 (2013) 328–338.

[61] B. Xue, J. Xu, C. Xu, R. Wu, Y. Li, K. Zhang, *Catal. Commun.* 12 (2010) 95–99.

[62] E.F. Iliopoulos, E. Heracleous, A. Delimitis, A.A. Lappas, *Appl. Catal. B Environ.* 145 (2014) 177–186.

[63] P.S.F. Mendes, F. Marques Mota, J.M. Silva, M.F. Ribeiro, A. Daudin, C. Bouchy, *Catal. Sci. Technol.* 7 (2017) 1095–1107.

[64] H. Toulhoat, P. Raybaud, E. Benazzi, *J. Catal.* 221 (2004) 500–509.

[65] M.Y. Kim, J.K. Kim, M.E. Lee, S. Lee, M. Choi, *ACS Catal.* 7 (2017) 6256–6267.